Research Letter DOI: 10.15541/jim20230462

# Spectroscopic Properties and Optical Clusters in Erbium-doped $CaF_2$, $SrF_2$ and $PbF_2$ Crystals

TAM YU Puy Mang[1,2], XU Yu[3], GAO Quanhao[1,2], ZHOU Haiqiong[1,2], ZHANG Zhen[4], YIN Hao[1,5], LI Zhen[1,2,5], LÜ Qitao[5], CHEN Zhenqiang[1,2,5], MA Fengkai[1,2], SU Liangbi[4]

(1. Guangdong Provincial Engineering Research Center of Crystal and Laser Technology, Department of Optoelectronic Engineering, Jinan University, Guangzhou 510632, China; 2. Guangdong Provincial Key Laboratory of Optical Fiber Sensing and Communications, Guangzhou 510632, China; 3. Analytical and Testing Center, Jinan University, Guangzhou 510632, China; 4. The State Key Lab of High Performance Ceramics and Superfine Microstructure, Shanghai Institute of Ceramics, Chinese Academy of Sciences, Shanghai 201899, China; 5. Guangdong Provincial Key Laboratory of Industrial Ultrashort Pulse Laser Technology, Shenzhen 518055, China)

**Abstract:** As a fundamental light source and a good window for atmospheric transmission, the mid-infrared 3 μm lasers have led many promising applications. The rare earth doped crystalline materials, such as erbium doped crystals, are some of the most important routes for generation of the lasers. However, they have an intrinsic shortcoming of self-termination because of their short lifetime of $^4I_{11/2}$ and longer lifetime of $^4I_{13/2}$. To eliminate this effect, a high concentration doping method is usually adopted to change the energy transfer process to decrease $^4I_{13/2}$ lifetime. The efficiency and output power of $Er^{3+}$-doped crystals were thus limited due to their degraded thermal properties. Trivalent erbium ions are easily clustering in fluoride crystals. Distances among the ions are short and therefore energy transfer processes could be significantly improved in the crystals even doping with low concentrations. Low doping concentrations could also alleviate the thermal effect in laser operations, which enable the erbium doped fluorides to be promising candidates for high power and high efficiency mid-infrared lasers. However, connection of spectral properties and erbium clusters is unknown. Here, the first principles calculation is utilized to model the erbium ion clusters in $CaF_2$, $SrF_2$ and $PbF_2$ crystals, concerning the absorption and photoluminescence properties. The results reveal that spectral properties and structures of the erbium clusters, evolve gradually with matrix crystals. Relationship between spectral properties and optical erbium clusters is determined qualitatively, which could be used to design new erbium doped mid-infrared lasers.

**Key words:** erbium; doping; mid-infrared laser crystal; erbium cluster; spectroscopic property

The mid-infrared 3 μm lasers have aroused significant interests due to a variety of applications in medical surgery, light sources for generation of far infrared wavelength lasers, infrared countermeasures[1-3], *etc*. As one of the most important routes, the rare earth doped crystalline lasers have been addressed. In particular, the $Er^{3+}$-doped mid-infrared lasers which can be directly pumped by the commercial laser diode (LD) have been extensively studied in fluoride, oxide and garnet crystals[4-7]. Due to the short lifetime of $^4I_{11/2}$ and longer lifetime of $^4I_{13/2}$, the heavy doping concentrations were generally adopted to remove the self-termination[8]. For example, more than 30% of $Er^{3+}$ ions were doped in garnet crystals to realize the population inversion[9]. However, the high concentration doping degenerates the thermal and mechanical properties and then laser performances of the crystal[10].

The trivalent rare earth ions are easily clustering in fluoride crystals and the distance between ions is greatly shortened[11-12]. It means that the intense energy transfer

**Received date:** 2023-10-09; **Revised date:** 2023-11-20; **Published online:** 2023-11-28
**Foundation item:** National Key R&D Program of China (2022YFB3605702); National Natural Science Foundation of China (61925508, 61905289); Key-area Research and Development Program of Guangdong Province (2020B090922006); Guangzhou Science and Technology Project (202201010427); CAS Project for Young Scientists in Basic Research (YSBR-024)
**Biography:** TAM YU Puy Mang (1997–), female, Master candidate. E-mail: pmtamyu@outlook.com
TAM YU Puy Mang (1997–), 女, 硕士研究生. E-mail: pmtamyu@outlook.com
**Corresponding author:** LI Zhen, professor. E-mail: ailz268@126.com; MA Fengkai, associate professor. E-mail: mafengkai@jnu.edu.cn
李 真, 教授. E-mail: ailz268@126.com; 马凤凯, 副教授. E-mail: mafengkai@jnu.edu.cn

among ions is highly expected even with very low doping concentrations. This is very beneficial for the $Er^{3+}$-doped mid-infrared lasers, in which the population inversion could be easily realized through the energy transfer processes[13-15]. The slope efficiency of 41.4% was obtained when doped with 4%$Er^{3+}$[16]. The continuous wave (CW) laser output power of 2 W was demonstrated in 1.3%$Er^{3+}$:$CaF_2$[17]. Even doped with 0.5%$Er^{3+}$, two orders of magnitude lower than that of $Er^{3+}$:YAG crystal, the CW efficiency of 20% was obtained[18]. These results suggest that the $Er^{3+}$-doped fluoride crystals are very promising candidates for generation of high efficiency high power mid-infrared lasers. Additionally, the erbium clusters contribute to the inhomogeneously broadened photoluminescence, then the tuning range of 123 nm was realized in the $Er^{3+}$-doped crystal[19]. The broad emissions also support the ultrafast mid-infrared lasers and the short pulses are highly expected[20].

The clusters are very important for the $Er^{3+}$-doped fluorides, however, the erbium clusters and the relationship with spectral properties are not clear, which hinders further exploring of the $Er^{3+}$-doped fluoride laser materials. In this work, spectral properties and the clusters of $Er^{3+}$-doped $CaF_2$, $SrF_2$ and $PbF_2$ were studied. It reveals that there exist two kinds of clusters, and concentrations of the centers are different, which leads to different spectral properties.

# 1 Experiment and simulation

The crystals of 1%$Er^{3+}$-doped (in atom) $CaF_2$, $SrF_2$ and $PbF_2$ were grown by the vertical Bridgeman method. For the as-grown crystals, the part near the seed was cut and double-face polished for the room temperature spectral measurement. The absorption spectra were detected with a Shimadzu UV-3600 ultraviolet-visible-near infrared (UV-VIS-NIR) spectrophotometer. The photoluminescence spectra were recorded by a FLS1000 time-resolved fluorimeter and the signals were collected by the red Photomultiplier Tube (PMT) under a Xenon lamp excitation. The erbium clusters were simulated by the Vienna *Ab-initio* Simulation Package (VASP)[21-22]. The plane-wave basis set and the projector augmented wave potential with Perdew-Burke-Ernzerhof (PAW_PBE) formula have been used[23]. The supercell size was 2×2×2 and only a Gamma k-grid was used to sampling the first Brillouin zone. The cut-off energy was set as 550 eV and the spin polarization was included. The convergence criteria were $10^{-5}$ eV and 0.01 eV·Å$^{-1}$ for the electronics and forces, respectively. The formation energy was obtained based on the methods in Ref. [24].

# 2 Results and discussion

Before discussions about the spectral properties, the energy level diagram of $Er^{3+}$ ions is sketched. $Er^{3+}$ ions could be efficiently pumped with a 980 nm LD, leading to a ~3 μm emission (Fig. 1). The energy transfer upconversion (ETU) process ($^4I_{13/2}$ + $^4I_{13/2}$→$^4I_{9/2}$ + $^4I_{15/2}$) among $Er^{3+}$ ions will deplete two photons from $^4I_{13/2}$ level and add one photon to the upper laser level $^4I_{11/2}$ by an additional nonradiative multiphonon relaxation (NMR) step, which is favorable for the ~3 μm lasing. The strong excited state absorption (ESA) process could also be observed in $Er^{3+}$ ions[25]. The particles on $^4I_{11/2}$ level were further excited to higher $^4F_{7/2}$ level, and the green light is emitted from $^2H_{11/2}$ and $^4S_{3/2}$ after a NMR process. The transition of $^2H_{11/2}$ to $^4I_{15/2}$ is spin forbidden and very weak intensity was expected[13]. As a comparison, the $^4S_{3/2}$→$^4I_{15/2}$ transition is spin allowed and $^4S_{3/2}$ is a metastable level, from which clear emission signals could be collected. More importantly, there are only two sublevels in $^4S_{3/2}$ when compared with that of $^2H_{11/2}$, $^4F_{9/2}$, $^4I_{11/2}$, $^4I_{13/2}$, and $^4I_{15/2}$, it means that the transitions from $^4S_{3/2}$ level would be easier to identify. The $^4S_{3/2}$→$^4I_{15/2}$ was therefore chosen and studied in the following sections.

The absorption spectra were firstly investigated and presented in Fig. 2. There exist three absorption lines at 520, 540 and 975 nm in the selected absorption range. The absorptions correspond to the intraconfigurational 4f-4f transitions of $Er^{3+}$ from its ground state to $^2H_{11/2}$, $^4S_{3/2}$ and $^4I_{11/2}$, respectively. Two absorption peaks can be observed in the transition of $^4I_{15/2}$→$^2H_{11/2}$, as well as that of $^4I_{15/2}$→$^4I_{11/2}$, and only one peak is observed for $^4I_{15/2}$→$^4S_{3/2}$. It can be seen that the absorption intensities and wavelengths varied with the crystals. The intensity

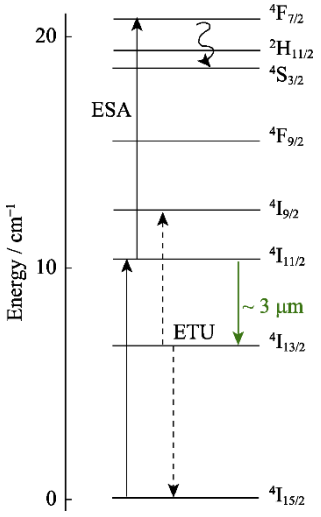


Fig. 1 Energy level diagram of $Er^{3+}$ ions

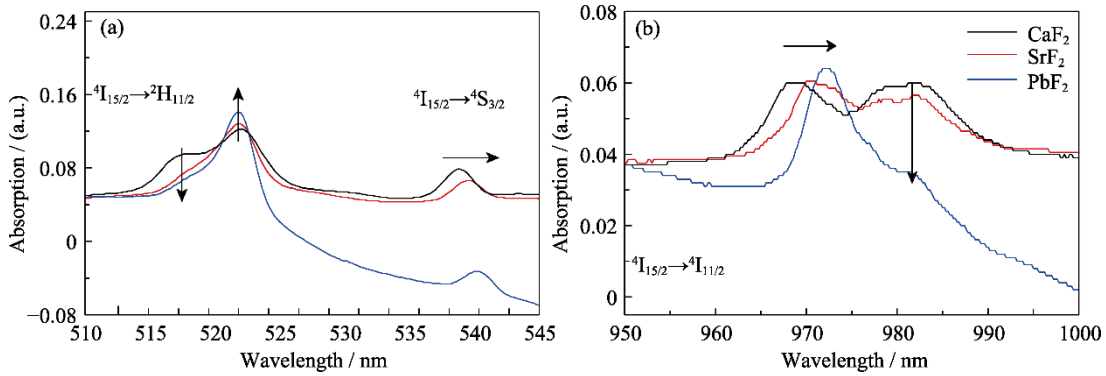


Fig. 2 Absorption spectra of $Er^{3+}$-doped $CaF_2$, $SrF_2$ and $PbF_2$ crystals
(a) $^4I_{15/2}\rightarrow{}^2H_{11/2}$; (b) $^4I_{15/2}\rightarrow{}^4I_{11/2}$; Colorful figures are available on website

of absorption at 517 nm decreases while that at 522 nm rises from $CaF_2$, $SrF_2$ to $PbF_2$, as the arrows denoted. Similarly, the absorption intensity of 981 nm decreases while that of 970 nm rises with increase of crystal cell sizes. Obviously, the absorptions of 970 and 981 nm, as well as that of 517 and 522 nm belong to different optical centers. The absorption wavelength of $Er^{3+}$:$CaF_2$ is 968 nm and shifts to 971 and 972 nm in $Er^{3+}$-doped $SrF_2$ and $PbF_2$, respectively, along with the red shift absorption of $^4I_{15/2}\rightarrow{}^4S_{3/2}$, which will be discussed in further.

The absorptions of 517 and 522 nm along with 519.5 nm were then chosen to excite the crystals. Since the transition rates of $^2H_{11/2}\rightarrow{}^4I_{15/2}$ are slow[26], which causes the weak intensity, and only emissions of $^4S_{3/2}\rightarrow{}^4I_{15/2}$ are presented. As can be seen in Fig. 3, the selectively excited emissions could be divided into three sections, A, B and C. The C emission lines are approximately parallel with each other under the three excitations in $CaF_2$, as well as that in $SrF_2$ and $PbF_2$, which indicates that the optical centers attributed to C emissions could be excited directly by the three wavelengths or indirectly through energy transfer. The normalized emission intensity of $Er^{3+}$:$PbF_2$ sample is higher when compared with that of $Er^{3+}$-doped $CaF_2$ and $SrF_2$. The content of optical centers for C emissions is expected to be larger in $Er^{3+}$:$PbF_2$. Compared with C emissions, B emission lines vary greatly with the excitations, especially in $CaF_2$ and $SrF_2$ crystals. The different emissions confirm that absorptions at 517 and 522 nm belong to different optical centers.

The A emission lines are also close to each other, similar to that of C lines, except the linewidths and peak wavelengths. The emission linewidth excited at 522 nm is sharply narrowed when compared with that at 517 nm. It suggests that more optical centers can be excited by 517 nm pumping which contributes to the broad emissions. It can also be seen that the emission wavelengths shift from 538.8 to 539.4 and 540.2 nm in going from $CaF_2$, $SrF_2$ to $PbF_2$. The red shifted emission wavelengths are in line with that of $^4I_{15/2}\rightarrow{}^4S_{3/2}$ absorptions in Fig. 2. It is noted that, as compared with $CaF_2$ and $SrF_2$ crystals, the emission line shapes under different excitations in $Er^{3+}$:$PbF_2$ are close to each other, the optical centers or local structures of the active ions in the crystal are probably the same.

The 522 nm excited emissions of the three crystals are also compared in Fig. 4. As can be seen, the intensity of B emission decreases while that of C rises from $CaF_2$,

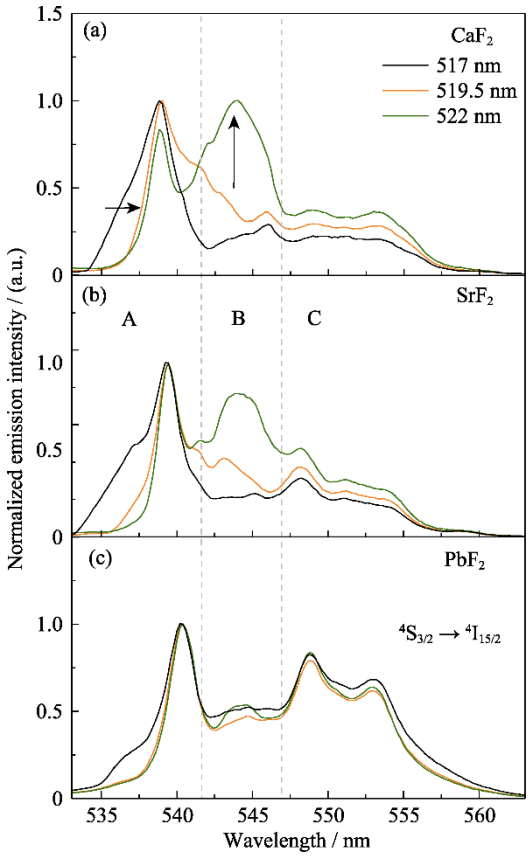


Fig. 3 Selective excited and height normalized emission spectra of $^4S_{3/2}\rightarrow{}^4I_{15/2}$ transition in $Er^{3+}$-doped fluoride
(a) $CaF_2$; (b) $SrF_2$; (c) $PbF_2$; Colorful figures are available on website

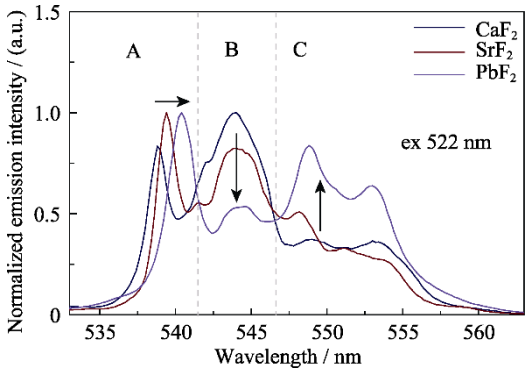


Fig. 4 Comparison of height normalized emission spectra of $Er^{3+}$-doped $CaF_2$, $SrF_2$ and $PbF_2$ excited at 522 nm

$SrF_2$ to $PbF_2$. Although the 522 nm excited emissions are different in the three crystals, however, based on the discussions about the absorption spectra, the 522 nm absorption is attributed to one group of centers. Two viewpoints should be addressed here. First, structures of the optical centers of 522 nm absorption depend on the matrix crystal, which evolves and varies with increase of lattice parameters. The evolved optical centers could be pumped simultaneously and give a radiative emission at 544 nm. Second, since the energy transfer processes are strong in the erbium clusters[18], the energy transfer assisted radiation could also lead to emissions in the band.

In order to have a clear description about the varied spectral properties, the erbium clusters are modeled and relaxed[11,27-28]. Formation energies and structures of the thermodynamic stable centers are listed in supplement of Table S1 and Fig. S1, the cluster symbols are based on Ref. [24]. It shows that the formation energy decreases as number of rare earth ions rises, which confirms the rare earth clustering in fluoride crystals[29]. There are sixteen kinds of erbium clusters in $Er^{3+}$:$CaF_2$, which is in well agreement with the site selective spectral results[30]. Those centers are divided into three groups, the monomers containing only one erbium ions, cubic sublattice centers and square antiprism structure clusters. Compared with erbium centers in $CaF_2$, stabilities of the monomer $1_1|0|0|1_1$ center and cubic sublattice centers are weakened in $Er^{3+}$:$SrF_2$, and such centers become unstable in $PbF_2$. At the same time, the transformation ability from cubic sublattice to square antiprism sublattice is strengthened. As can be seen, $3_1|0|6|4_1$ and $3_1|0|7|4_1$ with six and seven fluorines relaxed become $3_1|0|8|4_1$ with complete eight fluorines relaxed in going from $CaF_2$ to $SrF_2$. While for $PbF_2$ crystal, there are four and six fluorines relaxed even in the centers $1_1|0|4|2_1$ and $2_1|0|6|3_1$ containing only one and two erbium ions, respectively, which means that the transformation ability of $Er^{3+}$:$PbF_2$ is the strongest in the three crystals.

Number of erbium ions dependent formation energy is then depicted. It can be seen in Fig. 5, there exists an energy gap between the cubic sublattice and square antiprism structure clusters. Values of the energy gap rises from $CaF_2$, $SrF_2$ to $PbF_2$, which confirms the strengthened transformation ability. Nevertheless, the transformation from cubic to square antiprism sublattice is not instantaneous. Structures of the cubic sublattice and square antiprism sublattice clusters are gradually evolving and intimately related with the matrix crystals. That is why the 522 nm excited B emissions which belong to one group centers, evolve gradually with the varied matrix crystals. However, contributions from energy transfer processes to the varied emissions could not be absolutely ruled out.

Characteristics of the erbium clusters in $CaF_2$, $SrF_2$ and $PbF_2$ are thus clear. The erbium ions tend to form both the cubic sublattice and square antiprism structure clusters in $CaF_2$. As a comparison, stability of the cubic sublattice centers is weakened and that of square antiprism sublattice clusters rises in $SrF_2$. While for $PbF_2$, only square antiprism sublattice centers are thermodynamically stable. Although structures of the centers also depend on the doping concentrations, moderate doping level of 1% in the crystals could support the formation of cubic sublattice and square antiprism structure clusters[31]. Combined with the simulated cluster characters, it is known that the cubic sublattice centers contribute to 517 and 980 nm absorptions, and square antiprism sublattice clusters contribute to 522 and 970 nm absorptions. It should be noted that influences of the monomer centers are neglected. Since symmetries of the local structures in monomers are high, the forced electric dipole transition rates are very low which could be ignored as compared with that of high order clusters. Another question to be mentioned is the absorption and emission wavelengths shift. First, the varied crystal field splittings could lead to the shifted wavelengths. From $CaF_2$, $SrF_2$ to $PbF_2$, the transformation ability from cubic to square antiprism sublattice is enhanced and local symmetries around erbium ions are decreased from cubic to distorted tetragonal. The crystal field splittings are enlarged which contributes to the red shifted absorption and emission wavelengths. Second, the nephelauxetic effect is non-negligible[32]. Although anions in the crystals are the same, electronegativity of the lead is higher than that of calcium and strontium ions. $PbF_2$ is not a pure ionic crystal, and covalency effect could lead to the downshifted energy levels of erbium ions.

Based on the aforementioned discussions, it is known that erbium cluster structures are related with the matrix

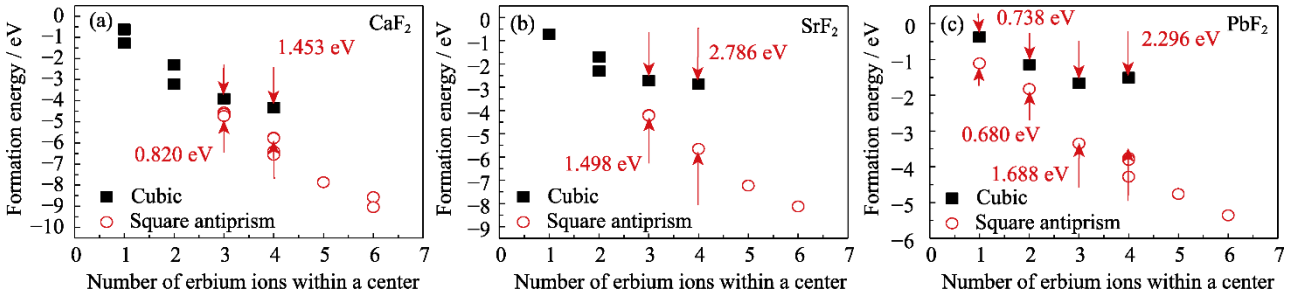


Fig. 5 Number of $Er^{3+}$ ions dependent formation energy of the clusters in fluoride
(a) $CaF_2$; (b) $SrF_2$; (c) $PbF_2$

crystals. In fact, not only matrix crystals, the rare earth ionic radii could also influence the cluster structures[11, 33]. Thermodynamic stability of the cubic sublattice clusters is weakened, and that of square antiprism structure clusters is increased from $La^{3+}$ to $Lu^{3+}$. Our previous results also reveal that the relative stabilities of cubic sublattice and square antiprism structure clusters are intimately related with that of monomer centers $1_1|0|0|1_1$ and $1_1|0|0|1_2$. If the $1_1|0|0|1_1$ with interstitial $F_i^-$ at the nearest site are more stable, the cubic sublattice centers are thus more stable; if the $1_1|0|0|1_2$ with interstitial $F_i^-$ at the next nearest site are more stable, the square antiprism structure clusters are more stable. There exists a critical line in which the stabilities of cubic and square antiprism sublattice clusters are equal. Critical line of $\Delta\mu$ = 0 eV is uncovered for the rare earth doped $CaF_2$ and $SrF_2$, and critical line of $\Delta\mu$ = 0.1 eV for the rare earth doped $BaF_2$[11,32]. $\Delta\mu$ is the formation energy difference between $1_1|0|0|1_1$ and $1_1|0|0|1_2$. Here critical line in rare earth doped $PbF_2$ is expected.

The $La^{3+}$, $Tb^{3+}$ and $Y^{3+}$ centers in $PbF_2$ are modeled and simulated as listed in supplement of Table S2 and Fig. S2. Compared with $1_1|0|0|1_1$, formation energy of $1_1|0|0|1_2$ is lower, which implies that the $1_1|0|0|1_2$ center in $La^{3+}$, $Tb^{3+}$ or $Y^{3+}$ doped $PbF_2$ crystal is more stable. The square antiprism structure clusters are therefore more stable in $Tb^{3+}$ or $Y^{3+}$ doped $PbF_2$. However, it can be seen that the cubic sublattice centers $2_1|0|1|2_1$, $2_1|0|1|3_1$, $3_1|0|1|3_1$, $3_1|0|2|4_1$ and $4_1|1|0|4_1$ are thermodynamically stable in $La^{3+}$-doped $PbF_2$, which indicates that $\Delta\mu$ = 0 eV is not the critical line in rare earth doped $PbF_2$. Number of rare earth ions dependent formation energy of the centers are then depicted in Fig. 6. A gap is observed between formation energy of the cubic and square antiprism sublattice centers, as the arrows denoted. Values of the gap are sharply increased from $La^{3+}$, $Tb^{3+}$ to $Y^{3+}$-doped $PbF_2$, which agrees well with the above discussions. It should be noted that formation energies of square antiprism sublattice clusters $3_1|0|8|4_1$ and $4_1|0|8|4_1$ are even higher than those of cubic sublattice centers $3_1|0|1|3_1$ and $4_1|1|0|4_1$ in $La^{3+}$:$PbF_2$, respectively. It is in contradiction with the results that formation energy of $1_1|0|0|1_2$ is lower about 0.1 eV as compared with $1_1|0|0|1_1$ center. It suggests that the critical value should be higher than 0.1 eV, which is adjusted to be 0.1–0.15 eV according to our previous work[11,32]. The critical line is depicted in Fig. 7. Since values of $\Delta\mu$ in $La^{3+}$, $Ce^{3+}$, $Pr^{3+}$ and $Nd^{3+}$ doped $PbF_2$ are around the critical line, it is reasonable to deem that cubic and square antiprism sublattice clusters would be coexisting in the crystals. And only square antiprism sublattice clusters are thermodynamically stable in the other rare earth doped $PbF_2$ crystals.

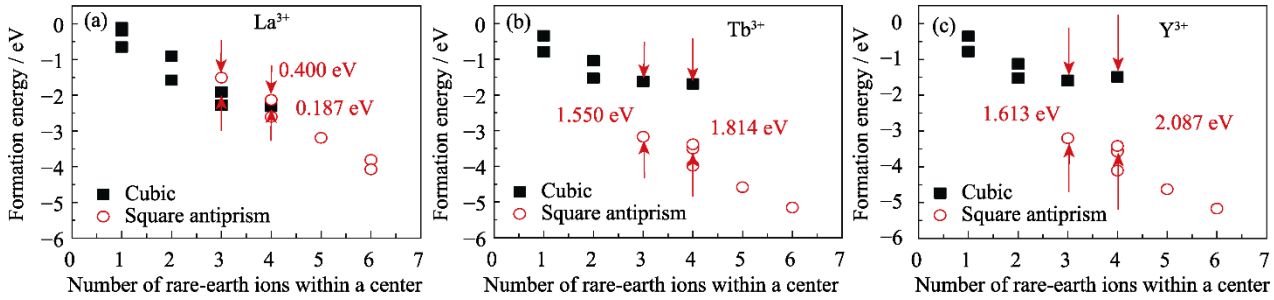


Fig. 6 Number of rare earth ions dependent formation energy of the clusters
(a) $La^{3+}$:$PbF_2$; (b) $Tb^{3+}$:$PbF_2$; (c) $Y^{3+}$:$PbF_2$

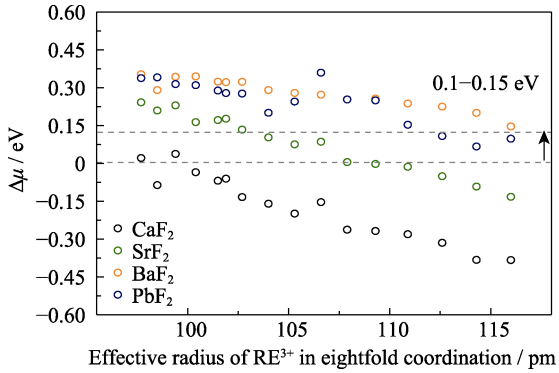


Fig. 7 Effective radius of $RE^{3+}$ dependent formation energy difference, $\Delta\mu$ between $1_1|0|0|1_1$ and $1_1|0|0|1_2$ center, $RE^{3+}$ includes $La^{3+}$ –$Lu^{3+}$ and $Y^{3+}$

## 3 Conclusions

Spectral properties of the $Er^{3+}$-doped samples vary greatly with matrix crystals. Simulation results and varied spectral properties reveal that structures of erbium clusters evolve gradually from $CaF_2$, $SrF_2$ to $PbF_2$. Stabilities of the cubic and square antiprism sublattice clusters in $Er^{3+}$:$CaF_2$ are comparable, which results in comparable absorptions of 517 and 522 nm, and of 970 and 980 nm, respectively. The square antiprism structure centers are more thermodynamically stable in $Er^{3+}$:$PbF_2$, absorptions of 522 and 970 nm then dominate the spectra. The relationship of spectral properties and optical clusters is then clarified qualitatively. It is very important for generation of mid-infrared lasers, especially the absorptions of 970 and 980 nm, suitable for commercial InGaAs LD pumping. The varied laser performances are highly expected when changing the pumping wavelengths. The relationship could also be used to design the needed spectral properties and then mid-infrared laser performances. Critical line of the centers is observed in rare earth doped $PbF_2$ crystal. The value is found to be 0.1–0.15 eV, larger than that of $CaF_2$, $SrF_2$ and $BaF_2$. Study on the differed critical values is on the way.

## Supporting information:

Supporting materials related to this article can be found at https://doi.org/10.15541/jim20230462.

### References:

[1] XUE Y Y, XU X D, SU L B, *et al*. Research progress of mid-infrared laser crystals. *Journal of Synthetic Crystals*, 2020, **49(8):** 1347.

[2] YANG J, ZHAO J B, LIU Y Y, *et al*. Near-infrared spectra and laser parameters of $Yb^{3+}$ and $Na^+$ codoped $CaF_2$-$SrF_2$ crystal. *Chinese Journal of Luminescence*, 2022, **43(3):** 341.

[3] YU T, ZHENG C Z, ZHAO S S, *et al*. Progress on application of Monte Carlo simulation in studying energy transfer mechanisms for rare-earth luminescent materials. *Chinese Journal of Luminescence*, 2022, **43(9):** 1390.

[4] DINERMAN B J, MOULTON P F. 3-μm CW laser operations in erbium-doped YSGG, GGG, and YAG. *Optics Letters*, 1994, **19:** 1143.

[5] KINTZ G J, ALLEN R, ESTEROWITZ L. CW and pulsed 2.8 μm laser emission from diode-pumped $Er^{3+}$:$LiYF_4$ at room temperature. *Applied Physics Letters*, 1987, **50:** 1553.

[6] MA F K, ZHANG Z, JIANG D P, *et al*. Cluster structure of rare earth doped fluorite halide crystals. *Journal of Synthetic Crystals*, 2023, **52(7):** 1219.

[7] ZHANG M, WANG G J, LIANG Y Y, *et al*. Continuous-wave laser properties of Er:$Lu_2O_3$ crystal grown by EFG method. *Chinese Journal of Luminescence*, 2023, **44(2):** 240.

[8] WU X, ZHANG Z, ZHANG Z H, *et al*. Laser-heated pedestal growth method and characterization of Er:YAP single crystal fibers. *Journal of Synthetic Crystals*, 2023, **52(7):** 1308.

[9] DONG K P, SUN D L, ZHANG H L, *et al*. Spectroscopy and LD end-pumped high power 2.79 μm CW laser from an Er:LuYSGG mixed crystal. *Journal of Luminescence*, 2021, **236(4):** 118107.

[10] YANG R, CHEN H R, TU L P, *et al*. Back energy transfer enhances $Er^{3+}$ upconversion luminescence. *Chinese Journal of Luminescence*, 2023, **44(9):** 1552.

[11] MA F K, SU F, ZHOU R F, *et al*. The defect aggregation of $RE^{3+}$ (RE = Y, La~Lu) in $MF_2$ (M = Ca, Sr, Ba) fluorites. *Materials Research Bulletin*, 2020, **125(5):** 110788.

[12] QIAN X Y, WANG W D, SONG Q S, *et al*. Luminescence property and Judd-Ofelt analysis of 0.6%Pr, *x*%La:$CaF_2$ crystals. *Journal of Inorganic Materials*, 2023, **38(3):** 357.

[13] ZHANG Z, MA F K, GUO X S, *et al*. Mid-infrared spectral properties and laser performance of $Er^{3+}$ doped $Ca_xSr_{1-x}F_2$ single crystals. *Optical Materials Express*, 2018, **8(12):** 3820.

[14] WANG H J, KOU H M, WANG Y Z, *et al*. Irradiation damage of $CaF_2$ with different yttrium concentrations under 193 nm laser. *Journal of Inorganic Materials*, 2023, **38(2):** 219.

[15] ZHAO X, LIU Z, LIN H, *et al*. Temperature sensing characteristics of $Y_7O_6F_9$:Er, Yb/PAN composite fibers based on up-conversion luminescence. *Chinese Journal of Luminescence*, 2023, **44(2):** 279.

[16] LIU J J, FENG X Y, FAN X W, *et al*. Efficient continuous-wave and passive Q-switched mode-locked $Er^{3+}$:$CaF_2$-$SrF_2$ lasers in the mid-infrared region. *Optics Letters*, 2018, **43(10):** 2418.

[17] ZONG M Y, ZHANG Z, LIU J J, *et al*. LD pumped high-power mid-infrared solid state lasers based on 1.3at%$Er^{3+}$:$CaF_2$ crystal. *Infrared and Laser Engineering*, 2021, **50:** 20210336.

[18] ZHANG Z, WU Q H, WANG Y X, *et al*. Efficient 2.76 μm continuous-wave laser in extremely lightly Er-doped $CaF_2$ single-crystal fiber. *Laser Physics Letters*, 2020, **17(8):** 085801.

[19] ŠVEJKAR R, ŠULC J, JELÍNKOVÁ H, *et al*. Diode-pumped Er:$SrF_2$ laser tunable at 2.7 μm. *Optical Materials Express*, 2018, **8:** 1025.

[20] WU G D, YIN X Q, FAN M D, *et al*. Nd-doped structurally disordered $YSr_3(PO_4)_3$ single crystal: growth and laser performances. *Journal of Rare Earths*, 2021, **39(12):** 1540.

[21] KRESSE G, FURTHMÜLLER J. Efficiency of *ab-initio* total energy calculations for metals and semiconductors using a plane-wave basis set. *Computational Materials Science*, 1996, **6:** 15.

[22] PERDEW J, BURKE K, ERNZERHOF M. Generalized gradient approximation made simple. *Physical Review Letters*, 1996, **77:** 3865.

[23] BLÖCHL P. Projector augmented-wave method. *Physical Review B*, 1994, **50:** 17953.

[24] MA F K, ZHOU H Q, TANG Q Y, *et al*. Clusters modification for tunable photoluminescence in $Nd^{3+}$:$SrF_2$ crystal. *Journal of Alloys and Compounds*, 2022, **899:** 162913.
[25] KOLOBKOVA E, NIKONOROV N, BABKINA A, *et al*. Concentration dependence of upconversion luminescence of $Er^{3+}$/$Yb^{3+}$ in the fluorophosphate glasses with small phosphates content. *Optical Materials*, 2020, **109(8):** 110279.
[26] TORQUATO A, OLIVEIRAS R A, SALES T O, *et al*. Influence of $PbF_2$ content on optical thermometry of $Er^{3+}$/$Yb^{3+}$ co-doped tungsten sodium phosphate glasses. *Optical Materials*, 2021, **112(12):** 110723.
[27] CORISH J, CATLOW C R A, JACOBS P W M, *et al*. Defect aggregation in anion-excess fluorites. Dopant monomers and dimers. *Physical Review B*, 1982, **25:** 6425.
[28] BENDALL P J, CATLOW C R A, CORISH J, *et al*. Defect aggregation in anion-excess fluorites II. Clusters containing more than two impurity atoms. *Journal of Solid State Chemistry*, 1984, **51:** 159.
[29] KAMINSKII A, ZHMUROVA Z, LOMONOV V, *et al*. Two stimulated emission $^4F_{3/2}\rightarrow{}^4I_{11/2,\ 13/2}$ channels of $Nd^{3+}$ ions in crystals of the $CaF_2$-$ScF_3$ system. *Physica Status Solidi A*, 1984, **84:** K81.
[30] TALLANT D R, WRIGHT J C. Selective laser excitation of charge compensated sites in $CaF_2$:$Er^{3+}$. *Journal of Chemical Physics*, 1975, **63:** 2074.
[31] MA F K, ZHANG Z, JIANG D P, *et al*. Neodymium cluster evolution in fluorite laser crystal: a combined DFT and synchrotron X-ray absorption fine structure study. *Crystal Growth & Design*, 2022, **22:** 4480.
[32] MA F K, ZHANG P X, SU L B, *et al*. The host driven local structures modulation towards broadband photoluminescence in neodymium-doped fluorite crystal. *Optical Materials*, 2021, **119(9):** 111322.
[33] CAI J J, MA C G, YIN M. Factors influencing the structure of the complex-defects in $AF_2$: $RE^{3+}$ (A=Ca, Sr and Ba): a first-principles study. *Journal of Luminescence*, 2022, **250(6):** 119058.

# 掺铒 $CaF_2$、$SrF_2$、$PbF_2$ 晶体的光谱性能与团簇结构研究

TAM YU Puy Mang[1,2], 徐 愉[3], 高泉浩[1,2], 周海琼[1,2], 张 振[4], 尹 浩[1,5], 李 真[1,2,5], 吕启涛[5], 陈振强[1,2,5], 马凤凯[1,2], 苏良碧[4]

(1. 暨南大学 光电工程系, 广东省晶体材料与激光技术工程研究中心, 广州 510632; 2. 广东省光纤传感与通信重点实验室, 广州 510632; 3. 暨南大学 分析测试中心, 广州 510632; 4. 中国科学院 上海硅酸盐研究所, 高性能陶瓷和超微结构国家重点实验室, 上海 201899; 5. 广东省工业超短脉冲激光技术重点实验室, 深圳 518055)

**摘 要:** 3 μm 波段中红外激光处于大气传输窗口, 又可以作为基础光源, 是激光技术研究的前沿。目前, 铒离子激活的激光晶体材料是产生 3 μm 中红外激光的重要途径之一。然而, $Er^{3+}$离子 $^4I_{11/2}$ 激光上能级荧光寿命较短, 下能级 $^4I_{13/2}$ 的寿命较长, 难以实现粒子数反转, 导致自终止现象。为了解决这一难题, 往往需要高浓度掺杂, 通过能量传递降低 $^4I_{13/2}$ 能级的寿命。然而高浓度掺杂又会造成晶体热性能变差, 限制了掺 $Er^{3+}$激光晶体效率和功率。三阶铒离子容易在氟化物晶体中形成团簇, 导致稀土离子间距缩短, 即使在低掺杂浓度下稀土离子之间的能量传递作用仍较为显著。同时, 低浓度掺杂还可以减轻激光运转下晶体的热堆积效应。掺铒氟化物晶体已成为一类重要的高功率、高效率中红外激光材料。然而, 掺铒氟化物晶体的光谱性能与铒离子团簇结构之间的相互联系尚不明确, 制约了掺铒氟化物晶体光谱和激光性能的进一步发展。本文采用第一性原理计算模拟了铒离子在 $CaF_2$、$SrF_2$ 和 $PbF_2$ 晶体中的团簇结构。结果显示, 铒离子团簇结构随基质晶体变化逐渐演变。结合模拟计算和实验表征定性揭示了不同晶体离子团簇与光谱性能的联系, 为掺铒氟化物中红外激光晶体材料的调控与设计提供参考。

**关 键 词:** 铒; 掺杂; 氟化物晶体; 铒离子团簇; 光谱性能

**中图分类号:** O77 **文献标志码:** A **文章编号:** 1000-324X(2024)03-0330-07

**Supporting information:**

# Spectroscopic Properties and Optical Clusters in Erbium-doped $CaF_2$, $SrF_2$ and $PbF_2$ Crystals

TAM YU Puy Mang[1,2], XU Yu[3], GAO Quanhao[1,2], ZHOU Haiqiong[1,2], ZHANG Zhen[4], YIN Hao[1,5], LI Zhen[1,2,5], LÜ Qitao[5], CHEN Zhenqiang[1,2,5], MA Fengkai[1,2], SU Liangbi[4]

(1. Guangdong Provincial Engineering Research Center of Crystal and Laser Technology, Department of Optoelectronic Engineering, Jinan University, Guangzhou 510632, China; 2. Guangdong Provincial Key Laboratory of Optical Fiber Sensing and Communications, Guangzhou 510632, China; 3. Analytical and Testing Center, Jinan University, Guangzhou 510632, China; 4. The State Key Lab of High Performance Ceramics and Superfine Microstructure, Shanghai Institute of Ceramics, Chinese Academy of Sciences, Shanghai 201899, China; 5. Guangdong Provincial Key Laboratory of Industrial Ultrashort Pulse Laser Technology, Shenzhen 518055, China)

**Table S1 Formation energy of $Er^{3+}$ clusters in $CaF_2$, $SrF_2$ and $PbF_2$**

| Symbol | Formation energy/eV | | |
|---|---|---|---|
| | $CaF_2$ | $SrF_2$ | $PbF_2$ |
| $1_1\|0\|0\|1_1$ | –0.637 | – | – |
| $1_1\|0\|0\|1_2$ | –0.624 | –0.725 | –0.371 |
| $1_1\|0\|1\|2_1$ | –1.272 | – | – |
| $1_1\|0\|4\|2_1$ | – | – | –1.109 |
| $2_1\|0\|2\|2_1$ | –2.305 | –1.700 | –1.145* |
| $2_1\|0\|3\|3_1$ | –3.214 | –2.308 | – |
| $2_1\|0\|6\|3_1$ | – | – | –1.825 |
| $3_1\|0\|1\|3_1$ | –3.909 | –2.722* | –1.662* |
| $3_1\|0\|5\|4_1$ | –4.729 | – | – |
| $3_1\|0\|8\|4_1$ | –4.555 | –4.200 | –3.350 |
| $3_1\|0\|8\|4_1$-C | –4.628 | –4.220 | – |
| $4_1\|1\|0\|4_1$ | –4.328* | –2.865* | –1.511* |
| $4_1\|0\|8\|4_1$-O | –5.749 | –5.651 | –3.754 |
| $4_1\|0\|8\|4_1$-A1 | –5.781 | –5.655 | –3.807 |
| $4_1\|0\|8\|5_1$-O | –6.407 | – | – |
| $4_1\|0\|8\|5_1$-A | –6.564 | – | –4.280 |
| $5_1\|0\|8\|5_1$ | –7.860 | –7.233 | –4.760 |
| $6_1\|0\|8\|5_1$ | –8.568 | –8.134 | –5.360 |
| $6_1\|0\|8\|6_1$ | –9.042 | – | – |

The values marked with asterisk means the center was thermodynamically unstable

**Table S2 Formation energy of the clusters in $La^{3+}$:$PbF_2$, $Tb^{3+}$:$PbF_2$ and $Y^{3+}$:$PbF_2$**

| Symbol | Formation energy/eV | | |
|---|---|---|---|
| | $La^{3+}$ | $Tb^{3+}$ | $Y^{3+}$ |
| $1_1\|0\|0\|1_1$ | –0.107 | – | – |
| $1_1\|0\|0\|1_2$ | –0.204 | –0.346 | –0.355 |
| $1_1\|0\|1\|2_1$ | –0.653 | –0.791 | – |
| $1_1\|0\|2\|2_1$ | – | – | –0.785 |
| $2_1\|0\|1\|2_1$ | –0.914 | – | – |
| $2_1\|0\|2\|2_1$ | – | –1.040 | –1.123 |
| $2_1\|0\|5\|3_1$ | – | –1.530 | –1.523 |
| $2_1\|0\|1\|3_1$ | –1.580 | – | – |
| $3_1\|0\|1\|3_1$ | –1.911 | –1.622* | –1.590* |
| $3_1\|0\|2\|4_1$ | –2.215 | – | – |
| $3_1\|0\|8\|4_1$ | –1.511* | –3.172 | –3.203 |
| $4_1\|1\|0\|4_1$ | –2.319 | –1.690* | –1.488* |
| $4_1\|0\|8\|4_1$-O | – | –3.452 | –3.542 |
| $4_1\|0\|8\|4_1$-A1 | – | –3.504 | –3.575 |
| $4_1\|0\|8\|4_1$-A2 | –2.132* | –3.383 | –3.417 |
| $4_1\|0\|8\|5_1$-A | –2.605 | –3.984 | –4.108 |
| $5_1\|0\|8\|5_1$ | –3.196 | –4.585 | –4.627 |
| $6_1\|0\|8\|5_1$ | –3.811 | –5.153 | –5.169 |
| $6_1\|0\|8\|6_1$ | –4.075 | – | – |

The values marked with asterisk means the center was thermodynamically unstable

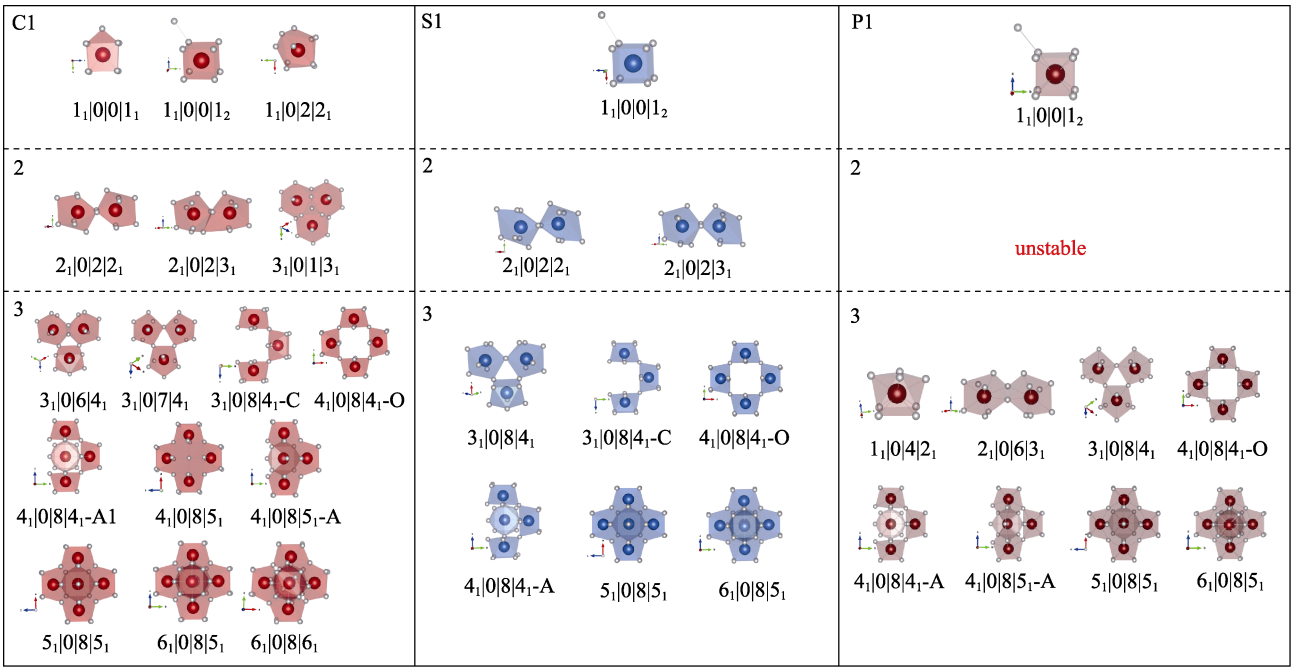


Fig. S1 Salculated thermodynamic stable centers of $Er^{3+}$ in fluoride (C) $CaF_2$; (S) $SrF_2$; (P) $PbF_2$
Centers are divided into three groups, the monomers, cubic sublattice clusters and square antiprism structure clusters which are denoted as "1", "2" and "3", respectively

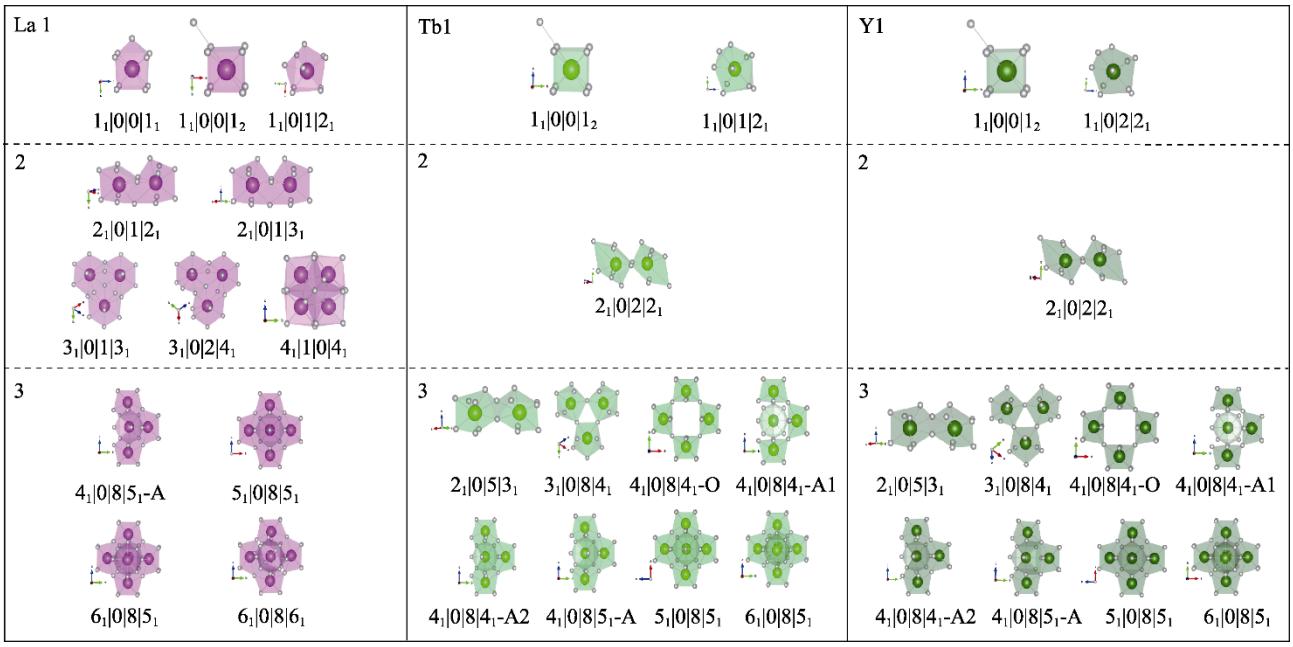


Fig. S2 Calculated thermodynamic stable centers in $PbF_2$ (La) $La^{3+}$; (Tb) $Tb^{3+}$; (Y) $Y^{3+}$